

Mechanism of surface influence on dislocation loop yield in copper and Cu₃Au

V. G. Kapinos

Department of Radiation Materials Science, Russian Research Centre "Kurchatov Institute," Moscow 123592, Russia

D. J. Bacon

Materials Science and Engineering, Department of Engineering, The University of Liverpool, Brownlow Hill, Liverpool L69 3GH, United Kingdom

(Received 20 November 1998)

A recently developed hybrid binary-collision/continuum model [V. G. Kapinos and D. J. Bacon, *Phys. Rev. B* **52**, 4029 (1995)] of temperature and defect evolution in displacement cascades has been used to investigate the influence of a nearby surface on vacancy defect formation in cascade events. The shape, vacancy, and thermal conditions in cascade zones that melt and intersect the surface during the thermal spike phase have been analyzed. Simplified geometries of such zones have been simulated by molecular dynamics on the basis of these data and the mechanisms of vacancy generation in the melt zone analyzed. It has been demonstrated that additional vacancies are formed in the resolidified zone under the surface through a combination of thermal sputtering and viscous flow of atoms from the cascade core. Quantitative relationships between the geometry and size of the melt zone and number of additional vacancies have been considered, and used in the hybrid model to calculate the depth, yield, and size distribution of vacancy dislocation loops in Cu and Cu₃Au irradiated with 50-keV Ni⁺ ions. The results are in good agreement with experimental data obtained by transmission electron microscopy of ion-irradiated thin foils. [S0163-1829(99)10329-1]

I. INTRODUCTION

Zones of reduced long-range order that are produced in irradiated ordered alloys by displacement cascades can be imaged in dark-field transmission electron microscopy of thin foils using suitable superlattice reflections.^{2,3} The shape and disposition of the disordered regions with respect to the irradiated surface can also be determined if stereo techniques are used. These methods have been used to characterize cascade damage in ordered alloys for disordered zones larger than the resolution limit involved in such microscopy. The advantage is that, in addition to the study of irradiation-induced disorder, vacancy dislocation loops formed by cascade collapse can also be analyzed as a result of their strain contrast. The fraction of cascades which collapse to loops, a quantity known as the "defect yield," can then be determined by detecting the presence of loop contrast in each zone. Muller *et al.*⁴ used this method recently to explore the effect of a nearby surface on cascade development and loop production in Ni₃Al and Cu₃Au alloys. This investigation was the first attempt to analyze experimentally the role of a surface in the process of vacancy dislocation loop formation in cascade damage.

The present investigation has been prompted by the results of recent molecular-dynamics (MD) computer simulations of near-surface cascades in gold by Averbach and co-workers.⁵⁻⁷ They observed that, in comparison with cascades in the bulk, damage production effects can be higher in a cascade just under the surface. They interpreted this effect as due to the melting of the cascade core during the thermal spike phase of cascade development and viscous flow of the resulting liquid onto the surface. The resolidified region under the surface contains more vacancies than the equivalent cascade core in the bulk and this increases the probability of vacancy clustering and loop formation. These authors concluded that experimental investigations of cascades using

heavy-ion damage of thin foils cannot be extrapolated to bulk damage conditions because the mechanism of depleted zone production in the bulk and near the surface are different.

Gao and Bacon⁸ have also demonstrated by MD simulation that the number of vacancies in disordered zones is increased in near-surface cascades and that this effect can lead to enhancement of vacancy clustering. Their results for Ni₃Al showed that the size of vacancy loops is directly proportional to the number of atoms emitted to the surface. However, for low-energy cascades (≤ 10 keV) almost all adatoms at the surface were found to be generated during the collisional phase rather than the thermal spike.⁸ Unfortunately, the number of cascades and maximum primary knock-on atom (PKA) energy in these MD simulations were too small to be compared directly with experiment. Thus the role of the thermal spike in the creation of adatoms through the mechanism of viscous flow of liquid from the melted core of a cascade is unclear, particularly for the high-energy cascades observed by transmission electron microscopy in thin foils. It is probable that this flow is one of several possible mechanisms that act simultaneously and influence the process of adatom formation in complex way. It is difficult to separate and investigate them in a systematic, statistical fashion using only MD simulation.

To overcome this problem and study the mechanisms in quantitative way, we propose in this work an approach where MD is applied for simplified geometries of the thermal spike. The use of such zones allows the results from a hybrid, binary-collision/continuum model of cascades to be employed.¹ The hybrid model explores cascade formation in energy and statistical regimes not open to direct MD simulation, and will be applied for consideration of the influence of a surface on vacancy loop production by high-energy cascades in Cu and Cu₃Au.

II. HYBRID MODEL SIMULATION

The hybrid model developed in Ref. 1 simulates the process of heat propagation in the cascade damage region, including absorption and creation of latent heat, melting, and the redistribution of density within the melt under the influence of the temperature gradient. The solution of the partial differential equation of heat conduction is used to describe the thermal spike stage. The material is described by a continuum, but the initial distributions of vacancies, interstitials, and temperature at the start of the thermal spike, are calculated by the MARLOWE binary-collision code.⁹ Electron-phonon coupling (EPC) is included in the model according to the methods proposed in Refs. 10 and 11. The value of the EPC strength parameter α_e for pure copper has been estimated in Ref. 10. An accurate value of α_e is not available for Cu₃Au and so we use the value for copper. Note that α_e for copper is predicted in Ref. 10 to be relatively small and so EPC does not have a significant effect on the results. The spatial electron temperature distribution in each of the subzones that form one cascade is defined by using sphere or cylinder approximations. The radius of a subzone is determined from the total number of melted cells, where each cell has dimensions a_0^3 , a_0 being the cube lattice parameter.

According to the model a vacancy loop is produced when a melted zone crystallizes if both the average concentration of vacancies and their total number exceed critical values C_v^{cr} and N_v^{cr} , respectively. The values of C_v^{cr} and N_v^{cr} for copper were extracted by comparison of hybrid-model calculations of vacancy loop yield and cascade efficiency with trends in experimental data obtained by transmission electron microscopy of ion-irradiated foils.¹ From this comparison it has been established that for nucleation of a vacancy loop in Cu the average vacancy concentration in the depleted zone has to achieve a level of more than 3–4 at. % and the number N_v^{cr} is equal to approximately 50 to 60. The value of these parameters was estimated from the direct MD simulation of the collapse of cascades in copper.¹¹ The influence of a nearby surface was not taken into consideration in these calculations and it was assumed that the vacancy loop yield obtained in the experiment represents the value in the bulk. That assumption is correct only if the number of zones affected by the surface is considerably smaller than the total number investigated.

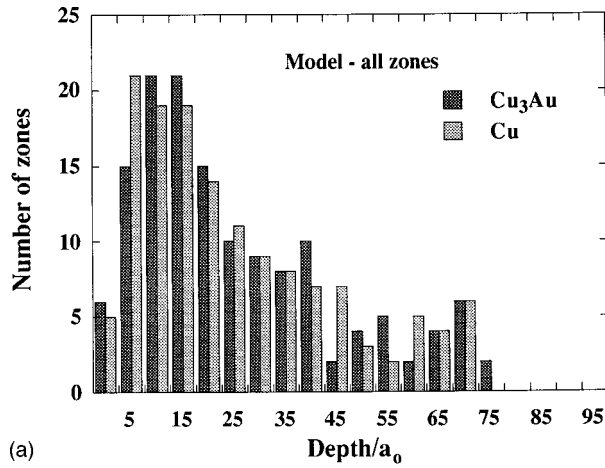
In Cu₃Au the defect yield is defined as the fraction of disordered zones containing a loop, and has the same meaning as in copper if there is a one-to-one correspondence between disordered zones and incident ions. The probability that a disordered zone contains a loop is dependent on the depth of the zone in the foil, but in the experiment⁴ the position of the foil surface was not determined precisely because no surface markers were present. We have used the hybrid model to calculate the distribution of molten zones with depth in Cu and Cu₃Au. For the ordered alloy, we assume that the disordered zone in the post-cascade state is the zone that melts during the thermal spike. (It has been shown in Ref. 12 that this provides a good fit between theory and experiment, and recent MD simulations of cascades in Ni₃Al support the correspondence between melt zone and disordered zone.⁸) The calculations allow zones to be identified

for which the mechanism of surface influence has to be applied.

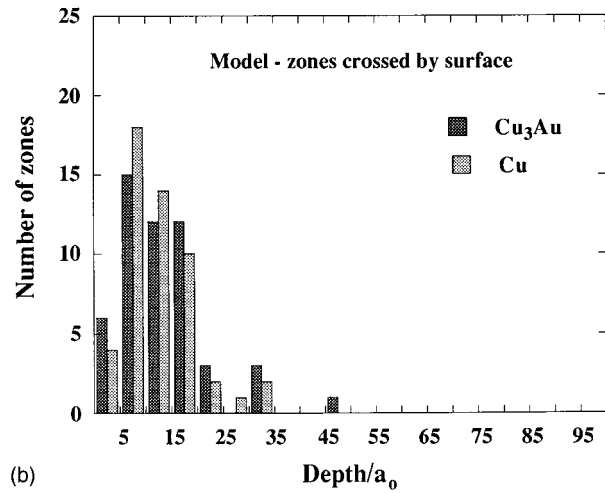
In the present work, approximately 100 cascades were simulated for both Cu and Cu₃Au in a foil of thickness $80a_0$ tilted at 45° to an incident beam of 50-keV Ni⁺ ions. This geometry reproduces the experimental irradiation condition used in Ref. 4, for which the tilt angle was selected in order to obtain detail on the shape of disordered zones along the ion-beam direction. The results of the calculation for the distribution of melted zones with depth are presented in Figs. 1(a) and (b). The depth is defined by the position of the center of gravity of the melted region measured along a normal from the surface. Figure 1(a) is for all zones and Fig. 1(b) is for those that actually reach the surface. The maximum number of zones crossed by the surface occurs at a depth of 10–20 a_0 (=4–7 nm) [Fig. 1(b)]. The calculated [Fig. 1(a)] and experimental [Fig. 1(b)] distributions of disordered zones for Cu₃Au have some differences. For example, the experimental distribution displays a maximum at a greater depth (~7.5 nm) than the calculated one (~5.6 nm), but this difference could be explained by the error (± 2 nm) in the location of the surface position in the experiment. A small population of zones is identified at a depth more than 20 nm in the theoretical histogram of Fig. 1(a), but not in the experimental distribution. It is possible that the thickness of the foil affects the contrast of disordered zones, reducing their projected size on the image plane of the microscope.¹²

Now we consider some parameters that characterize the zones intersected by the surface. Figure 2 shows the distribution of the average temperature \bar{T} and vacancy concentration \bar{C}_v in the melt of the 52 such zones in Cu₃Au at the end of ballistic stage. The value of \bar{C}_v was determined according to the model of density redistribution described in Ref. 1. The record of these parameters was taken at the moment when the size of the melt achieved its maximum value. It is seen that \bar{T} and \bar{C}_v lie in the range 5000–10 000 K and 0.4–1.1 at. %, respectively. Another important parameter for a zone crossed by the surface is the number of melted cells (of area a_0^2) at the surface. This number allows the average size of the melted area at the surface to be estimated and will be used later for calculation of the number of additional vacancies in the melted and crystallized core (see next section). The distribution of the number of melted surface cells in Cu₃Au is plotted in Fig. 3. It is seen that the average radius \bar{R} of the melted “spot” on the surface lies in the range 3–5 a_0 . Figure 4 shows the distribution of average depth \bar{L} of the liquid for molten zones crossed by the surface. This parameter was estimated as follows. For each melted cell at the surface, the length of the continuous chain of nearest-neighbor melted cells along the normal to the surface was found, and the average length of all such cells for each zone was calculated. It is seen from Fig. 4 that the average value \bar{L} has a maximum located at about 6–8 a_0 .

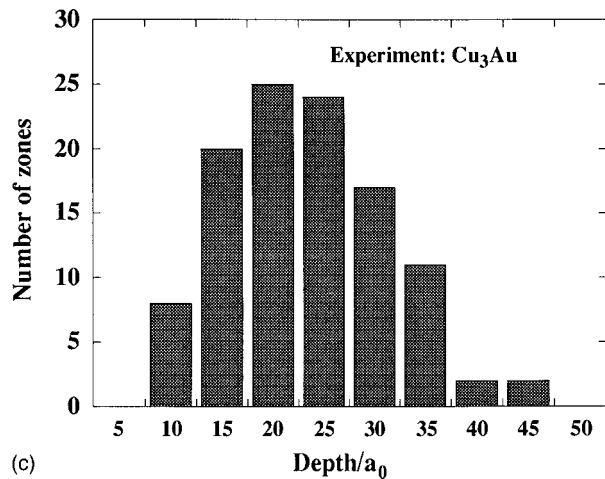
Analysis of the shape of these zones in the layers closest to the surface shows that it is cylindrical, on average, with its axis inclined at 45° to the surface. To demonstrate this, consider the ratio N_{in}/N_{out} for each zone, where N_{in} and N_{out} are \bar{T} calculated according to the following procedure. The



(a)



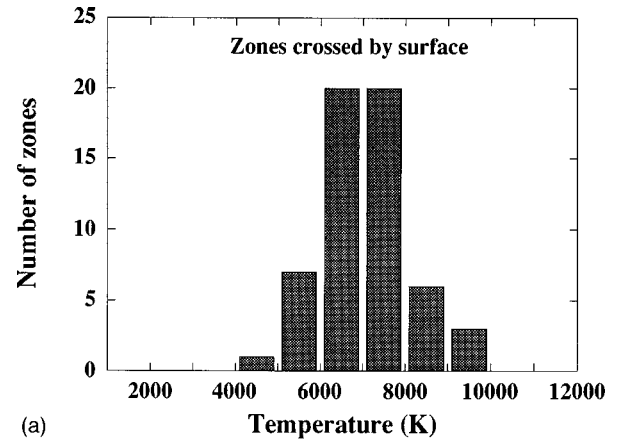
(b)



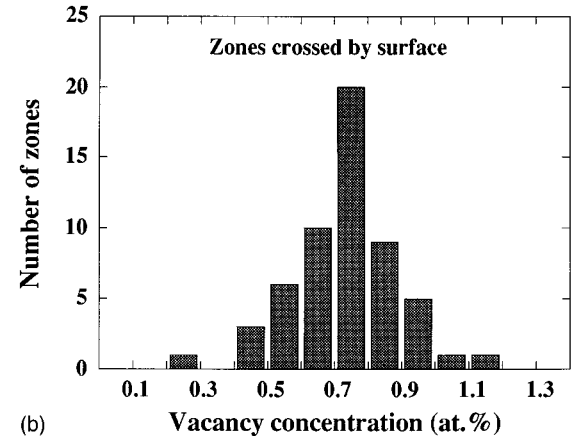
(c)

FIG. 1. The number of disordered zones in Cu₃Au irradiated with 50-keV Ni⁺ ions at an incident angle of 45° as a function of the depth in the foil. The results obtained by the hybrid model are shown in (a) and (b) and those found by experiment (Ref. 4) are in (c).

melted cells in the plane (001) at a particular depth are selected and defined to be N_{tot} . The number of cells in the same plane but having a direct connection along the [001] direction through the liquid to a melted cell on the surface are defined to be N_{in} . The difference ($N_{out} - N_{in}$) is equal to N_{out} . The value of N_{in}/N_{out} averaged over all zones with \bar{R}



(a)



(b)

FIG. 2. Distributions of (a) the initial temperature \bar{T} and (b) the vacancy concentration \bar{C}_v averaged over 52 melted subzones in Cu₃Au. The results are for zones crossed by the surface.

equal to either $2a_0$ or $4a_0$, as given by the data of Fig. 3, is plotted as a function of distance from the surface in Fig. 5. The same ratio for the same zones but assuming that they have cylindrical shape and are crossed by the surface at an angle of 45° was also calculated, the area of cylinder being determined from the number of cells at the surface. These

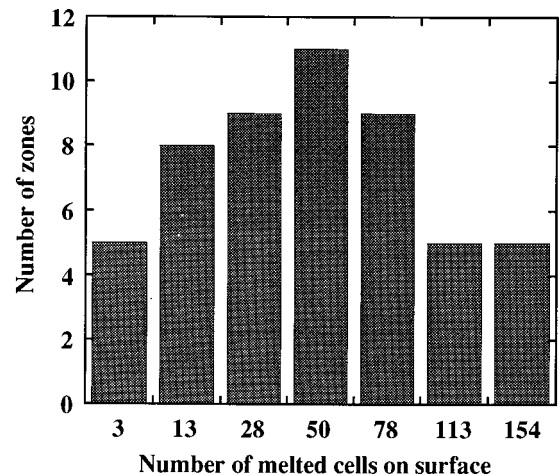


FIG. 3. Distribution of the number of melted cells on the surface for 52 melted subzones in Cu₃Au. The area of each cell is equal to a_0^2 , where a_0 is the lattice parameter.

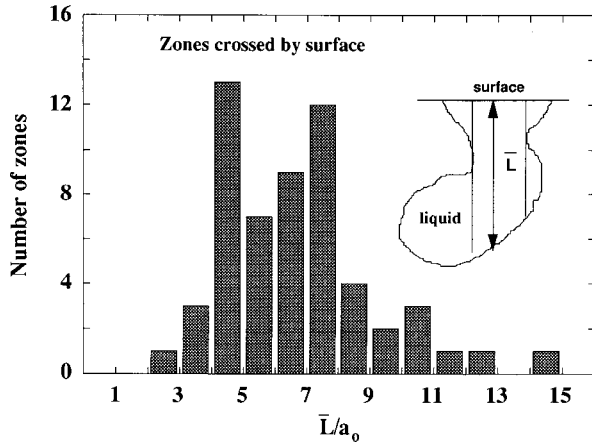


FIG. 4. The distribution of average depth \bar{L} of the liquid region defined as in the inset figure.

calculations are also displayed in the figure. The cylinder approximation can be applied only for the near-surface parts of zones. To estimate the depth over which this is so, we calculated the ratio $\bar{L}/2\bar{R}$ for each zone, where the average depth has been taken from Fig. 4, and the average size of the melted spot at the surface \bar{R} was estimated from Fig. 3. The results of calculation of the ratio averaged over all 52 zones are presented in Fig. 6 as a function of \bar{R} . For cylindrical zones inclined at 45° to the surface, the ratio is expected to be close to unity. It is seen that the cylinder shape exists only for \bar{R} less than $5a_0$ on average. The zones with \bar{R} more than $6a_0$ tend to have a shape similar to a segment of a sphere because $2\bar{R}$ is approximately three times \bar{L} . These results on shape are expected to change with ion energy.

III. MD SIMULATION OF THE THERMAL SPIKE NEAR THE SURFACE

A. Method

The real temperature distribution in a thermal spike gives a melted region of irregular shape and it is necessary to use

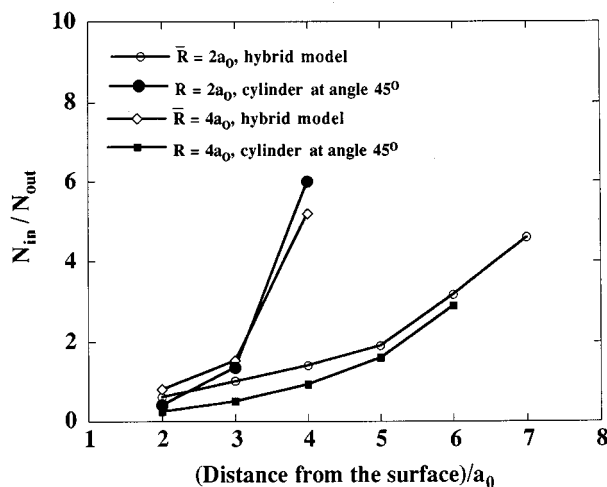


FIG. 5. The ratio N_{in}/N_{out} plotted as a function of a distance from the surface (see text).

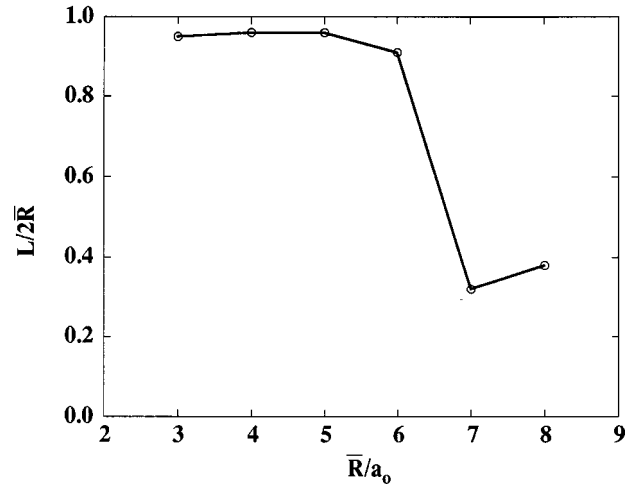


FIG. 6. The ratio $\bar{L}/2\bar{R}$ plotted as a function of average radius \bar{R} of the melted spot on the surface. The value of \bar{R} has been estimated from the number of cells on the surface (Fig. 3). The average depth \bar{L} has been taken from Fig. 4.

much computing resource to simulate a statistically representative number of configurations by MD for high-energy cascades. The real geometry of cascades can be simulated effectively within the approximation of the hybrid model. However, MD simulation can be used to introduce the necessary relationships into the hybrid model in order to calculate the surface influence on vacancy loop yield. To investigate the mechanisms in a systematic manner, simplified geometries of the thermal spike and depleted, vacancy-rich zones have been considered. Most of the results have been obtained for a thermal spike with cylindrical geometry. The length, radius, and angle of inclination of the cylinder to the surface (0° and 45°) are the variable parameters. A number of atoms N_v was randomly removed from the cylindrical region to simulate the depleted zone to provide an average vacancy concentration equal to a specified quantity \bar{C}_v .

The energy dissipation process and structural evolution in the thermal spike was simulated in an MD cell with 122 500 movable atoms in the fcc crystal structure and surface normal along [001]. The dimensions were $35a_0 \times 35a_0 \times 25a_0$. The cell had rigid boundaries along [100] and [010] and a periodic boundary condition along [001]. The MD timestep t_0 was taken to be 4 fs. A thermal spike was introduced at zero time with an uniform temperature distribution within the depleted zone. After a time of ~ 0.1 – 0.2 ps, the thermalization process was almost complete and a Gaussian-like temperature profile was established. The temperature in the melted part of the zone was characterized by the average temperature T . As a consequence of thermal expansion, large fluctuations of pressure and temperature appeared in the cell. To dampen the influence of the waves reflected from the boundaries, a special procedure was used based on freezing the position of the atoms in a few layers adjoining the rigid boundaries of the cell along the x and y axes. From the hybrid model calculations, the initial spike temperature is in the region of 5000–10 000 K for Cu_3Au irradiated by 50-keV Ni^+ ions [see Fig. 2(a)]. Thus, for the MD calculations, we selected three initial temperatures of 5000, 7000, and 9000

K. The simulations were carried out for one model representing both metals. We used the many-body interatomic potential for copper derived in Ref. 13, but modified as described in Ref. 14 to reproduce the pressure-volume relationship of single crystals and provide better treatment of interactions inside the normal nearest-neighbor distance between atoms.

The length L and radius R of the cylinder used to mimic the cascade core region were chosen to be in the ranges $2-8a_0$ and $2-6a_0$, respectively. To demonstrate the influence of irregularity on the results we used various shapes of the thermal spike based on the cylinder geometry, as described below, and, for a few cases, spikes with spherical geometry were also considered.

B. Results

Figure 7 shows the $[010]$ projection of atoms in the central part of the MD cell at (a) the beginning ($t=100t_0$) and (b) the end ($t=3000t_0$) of the thermal spike. The initial concentration and temperature of the depleted, cylindrical zone were 1 at. % and 9000 K, respectively. The cylinder length and the radius were $8a_0$ and $4a_0$, respectively, and the cylinder axis was at 45° to the surface normal. It is seen that the spike has formed a crater, created additional atoms ('adatoms') at the surface and sputtered atoms off the surface. (The sputtered atoms are captured at the lower surface of the block, which is formed by applying the periodic boundary condition along $[001]$.) The figure thereby demonstrates typical mechanisms by which the surface influences vacancy loop formation. The additional number of vacancies N_{add}^V which remain in the crystal and form an extended defect can be calculated by the formula

$$N_{\text{add}}^V = N_{\text{sputt}} + N_{\text{add}}^i - N_{\text{crat}}, \quad (1)$$

where N_{sputt} is the number of sputtered atoms, N_{add}^i is the number of adatoms formed at the surface, and N_{crat} is the number of lattice sites forming the crater. The values of N_{sputt} , N_{add}^i , and N_{crat} are dependent on the initial values of C_v , T , L , R , and the shape of the depleted zone. The influence of all of these parameters has been investigated.

When the melted zones achieve their maximum size, they have an average concentration of vacancies in the range 0.4–1.5 at. % (Sec. II). We have therefore investigated this parameter in the range 0.5–2.0 at. %, and find that the influence of \bar{C}_v on the parameters in Eq. (1) is small. As an example, Fig. 8 demonstrates the data for the number of adatoms N_{add}^i as a function of \bar{C}_v for different radii of cylinder. These data were obtained for $T=7000$ K and $L=8a_0$, and the cylinder axis was at 45° to $[001]$. Because of the small sensitivity of N_{add}^i to changes in \bar{C}_v , we used only one typical value of \bar{C}_v in the remaining simulations: it was chosen to be 1 at. %.

The dependence of N_{sputt} , N_{add}^i , and N_{crat} on the initial temperature of the spike is shown in Fig. 9. These calculations were conducted for a cylinder of length $8a_0$ and values of R in the range $3-5a_0$ and inclined at 45° to the surface. The number of additional vacancies N_{add}^V calculated by Eq. (1) is also shown. It is seen that the first three parameters increase with increasing spike temperature, although no atoms were sputtered from the surface at the lowest temperature in these simulations. The number of additional vacancies

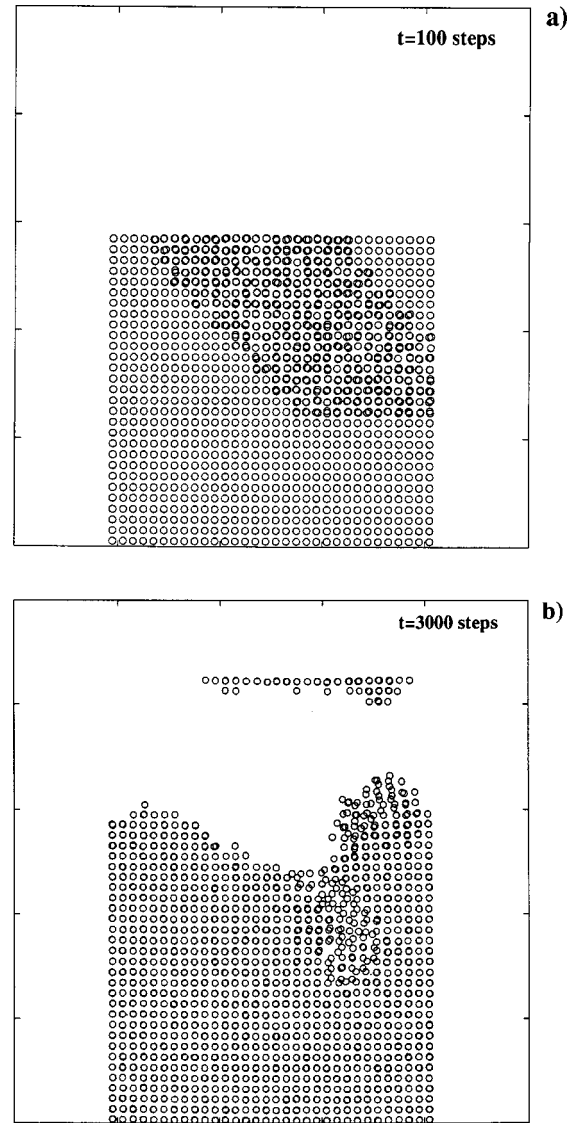


FIG. 7. Positions of atoms within a (010) cross-sectional slab, $2a_0$ thick, at times (a) $100t_0$, and (b) $3000t_0$. Initially the temperature was 9000 K and was distributed within a cylinder of length $8a_0$. The cylinder radius was $4a_0$ and the axis was 45° away from the normal to the surface. The sputtered atoms are captured at the under surface formed as a result of applying the periodic boundary condition along $[001]$.

increases only for the smallest radius ($R=3a_0$) and is insensitive to the temperature for larger radii. The nonzero value of N_{add}^V was found to occur only when $L>4a_0$, and for long enough cylinders these extra vacancies formed a dislocation loop or extended cluster under the bottom of the crater.

The mechanism of formation of these extended defects is the result of two processes. First, there is the fast evaporation of atoms from the melted atomic layers nearest to the surface. (Note that the data for N_{sputt} cannot be compared directly with experiment because they only apply to molten zones that intersect the surface.) For small R , the creation of these sputtered atoms forms a crater on the surface with a shape resembling a pyramid. A similar structure was noticed by Gao and Bacon⁸ in the direct MD simulation of a 10-keV cascade under the surface of Ni_3Al . The depth of craters is a function of cylinder radius and initial temperature. The sec-

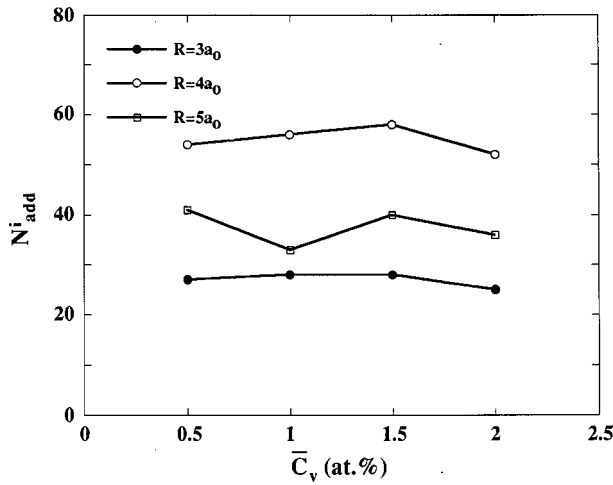


FIG. 8. Data for the number of adatoms N_{add}^i as a function of average vacancy concentration \bar{C}_v in the melted zones with different cylindrical radii. These data were obtained for $T=7000$ K and $L=8a_0$, and the cylinder axis was at 45° to the normal to the surface.

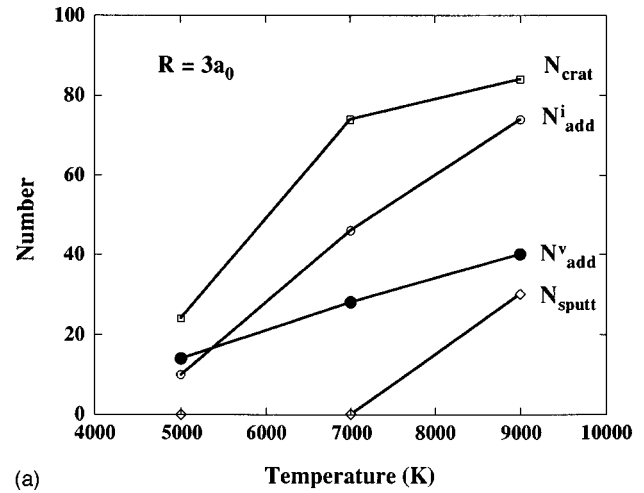
ond process is the liquid flow to the surface stimulated by the formation of high internal pressure in the melt. Part of the crater is filled with atoms during this movement of liquid and excess vacancies are created during solidification near the crater bottom, thereby forming a vacancy cluster. The first process dominates if the cylinder is short ($L \leq 3-4a_0$) and has a radius less than $3-4a_0$. In this case the final structure consists only of a crater.

C. Investigation of zone geometry

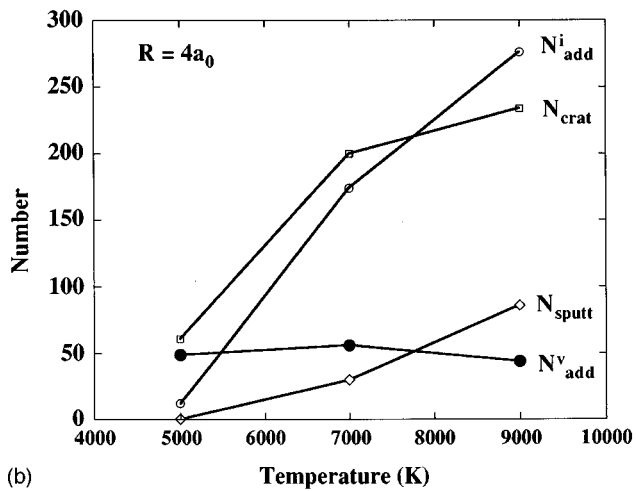
The results above were obtained for a cylindrical geometry of the melted zone, as illustrated schematically in part E of Fig. 10. On average, this geometry describes the shape of the melted zones in layers near the surface. Real zones have irregular shape and that may influence the values of the parameters used in Eq. (1). To estimate their sensitivity to variations in shape of the melted zone, a few MD simulations were also carried out on crystals with different initial configurations of the thermal spike, an example of which is depicted in part F of Fig. 10. However, these suggested that the quantitative defect data are insensitive to shape of the molten zone in layers well below the surface and are more strongly influenced by the size of the melted spot at the surface and the depth over which the cylindrical approximation to shape applies. Thus to investigate the influence of zone geometry in a systematic manner, the simplified zone forms sketched in parts A–D of Fig. 10 were simulated.

Consider the configurations labeled B and C, which are zones consisting of two joined cylinders. The upper cylinder has radius R and the lower one has radius $R+R_h$ (zone B) or $R-R_h$ (zone C). The length of second cylinder is equal to h . Figures 11(a) and (b) demonstrate the variation of number of adatoms N_{add}^i as a function of parameter h for configuration B and C, respectively. In these examples, the overall depth of the molten zone and the initial temperature were $11a_0$ and 5000 K, respectively.

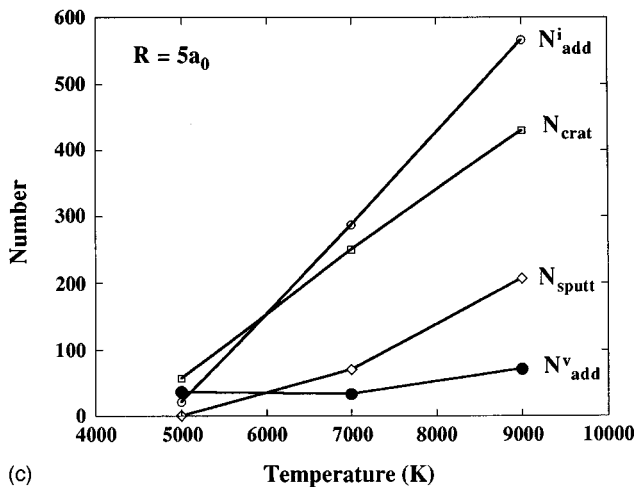
It is seen for the B configuration that if the value of h is small (less than about $8a_0$), the number of adatoms does not



(a)



(b)



(c)

FIG. 9. Data for the number of lattice sites in the crater N_{crat} , the number of adatoms N_{add}^i , the number of sputtered atoms N_{sputt} , and the number of additional vacancies $N_{\text{v_add}}^i$ as a function of the initial temperature in the thermal spike. The cylindrical thermal spike had a length $L=8a_0$ and a radius of either (a) $3a_0$, (b) $4a_0$, or (c) $5a_0$, and the cylinder was at 45° to the normal to the surface.

depend on h . This means that the number of atoms crossing the surface plane depends mainly on the size $2R$ of the melted spot at the surface. If that size is not influenced by the shape of the melted zone, the number N_{add}^i is almost con-

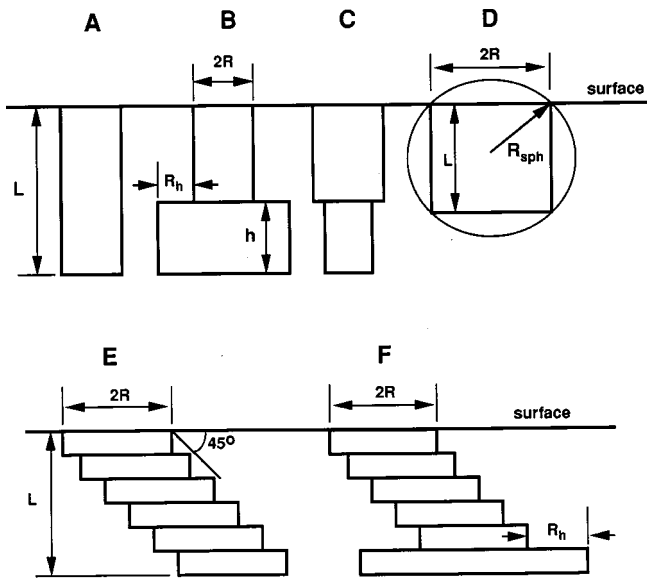
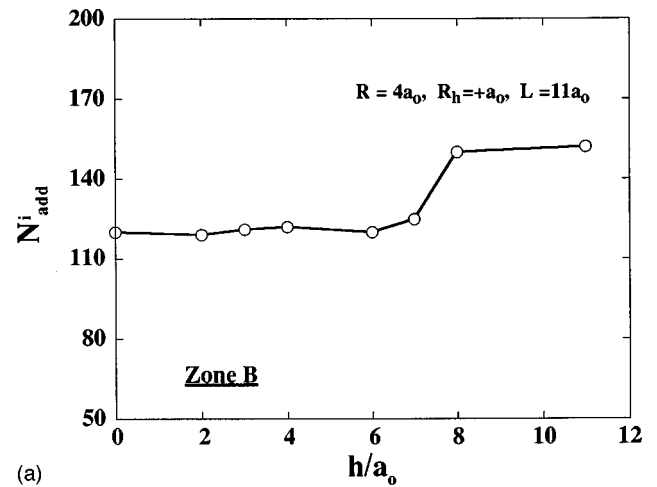


FIG. 10. Schematic illustration of the configurations of the thermal spike investigated by MD.

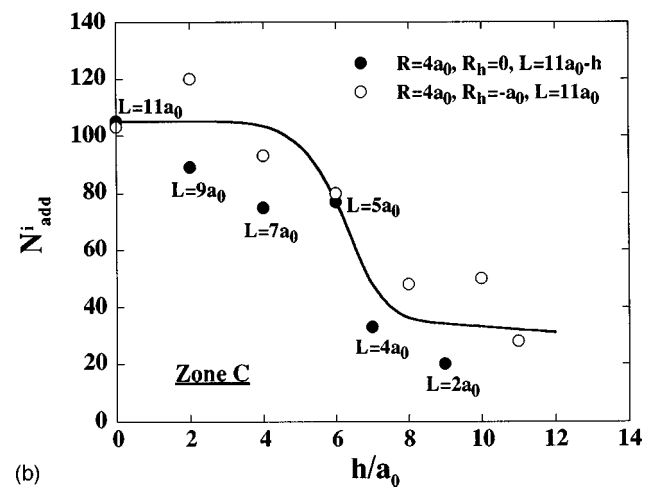
stant. For the example of the zone geometry depicted by B, the size of the melted spot at the surface can be changed if h is more than about $8a_0$, and this results in an increase in N_{add}^i [see Fig. 11(a)]. To analyze the results of the calculations for the C configuration, we compare N_{add}^i with similar data obtained for the simple cylinder geometry (zone A), which has the same radius and length as the upper part of zone C. The results for these C and A geometries are presented in Fig. 11(b) by open and filled circles, respectively. It is seen that, as for the B configuration, the number of adatoms is influenced mainly by the size of the melted area at the surface, rather than the geometric shape lower down. It is interesting that the simple cylinder (open circles) reproduces the data for the C geometry for the whole range of values of h considered.

We also investigated the validity of the cylinder approximation for describing the number of adatoms created by a melted spherical zone crossed by the surface (configuration D in Fig. 10). The number of adatoms for the sphere was compared with the number obtained for a cylinder crossed by the surface. The radius of the cylinder R was set equal to the radius of the circle formed by the intersection of the surface plane with the sphere. The length L of cylinder was equal to the length of the liquid column under the cross section (see Fig. 10). It was found that the number of adatoms for the two geometries are in very good agreement. This is illustrated in Fig. 12, where N_{add}^i is plotted against the height of the sphere outside of the surface, $R_{\text{sph}} - L/2$, and the solid and dashed lines are the dependencies for the sphere and cylinder geometry, respectively. The results were derived for zones with spherical radii of either 4 or $5a_0$, as indicated, and the initial temperature was 5000 K. It is seen that the number of adatoms depends mainly on the area of liquid at the surface and the length of tube of liquid under it.

There are regions of maximum pressure in the tube of liquid far from the surface which are developed due to the change in the melted volume.⁶ The pressure falls to zero at the surface and that defines the number of atoms passing



(a)



(b)

FIG. 11. Variation of the number of adatoms as a function of parameter h for configurations (a) B and (b) C of Fig. 10 by MD simulation with $L = 11a_0$. The open circles are the results obtained for B with $R_h = +a_0$ and C with $R_h = -a_0$. The filled circles in (b) are the results estimated from the calculations for configuration A of Fig. 10 with the length of cylinder equal to $L - h$.

through the surface [see Eq. (2) below]. Using MD simulation of a thermal spike, it has been demonstrated that the maximum pressure in the melt is uniform.¹⁷ This means that the shape of the melted region far from the surface has minor influence on the value of the maximum pressure.

D. Comparison with the viscous flow model

Averback and Ghaly have proposed a macroscopic model of surface melting, according to which, for an infinite cylinder crossed by the surface, the number of atoms Q passing through the surface is described by the formula⁶

$$Q = (\pi\rho\Delta\rho\Delta P/32\mu D)^{1/2}R^4, \quad (2)$$

where R is the maximum radius of the liquid cylinder, $\Delta\rho$ is the difference in atomic densities in the melt and solid, ΔP is the drop in pressure from the interior of the cylinder to the free surface of the liquid, μ is the viscosity of the liquid, and D is the thermal diffusivity. It is of interest to compare our MD results with Eq. (2) in a qualitative way without definition of the absolute magnitudes from Eq. (2). According to

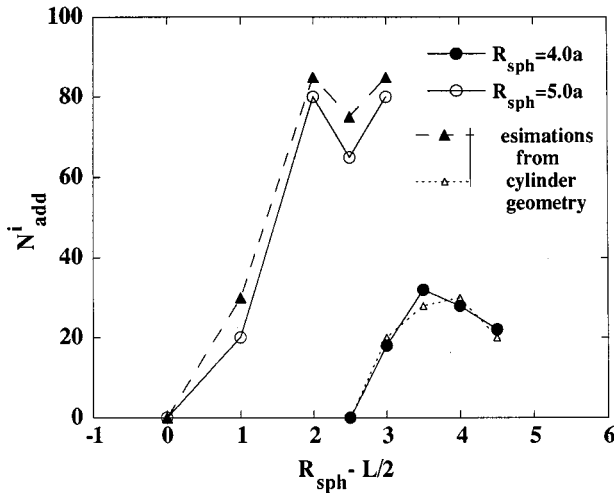


FIG. 12. Data showing the result of applying the cylinder approximation for the description of a spherical melted zone that intersects the surface, as illustrated in configuration D of Fig. 10.

our calculations (see Fig. 9), Eq. (2) applies in the temperature regime 5000–6000 K where the mechanism of viscous flow dominates and the number of sputtered atoms is small. MD simulations were therefore conducted for $T = 5000$ K for cylinders with different radii and lengths. The results are shown in Fig. 13 as the number of adatoms versus R^4 for the cylindrical thermal spike depicted as A in Fig. 10. It is seen that Eq. (2) does not describe all the MD results by one curve. For cylinders with $R < 4.5a_0$ (i.e., $R^4 < 410a_0^4$) and L in the range $7-11a_0$ the model represented by Eq. (2) gives a satisfactory description. For cylinders with $L = 7-11a_0$ and $R > 4.5a_0$ (ratio $R/L > 0.6$), the size of the melted spot at the surface becomes comparable with the length of the cylinder. In that case, the mechanism of crater formation becomes important and that decreases the number of adatoms. It is of interest that the data for short cylinders ($L \leq 5a_0$) are also

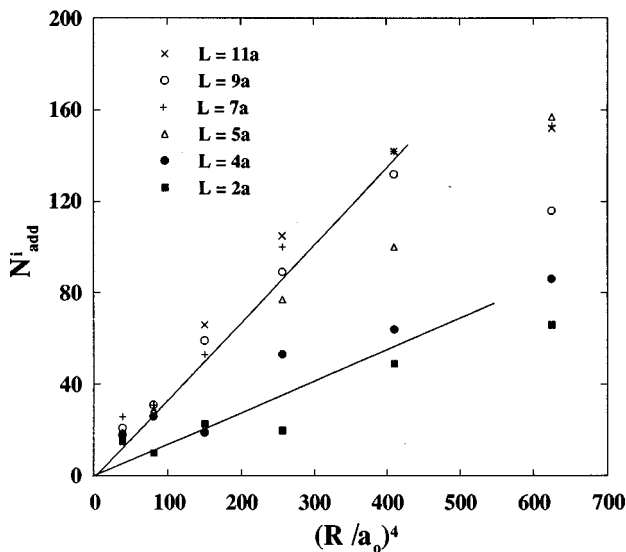


FIG. 13. Variation of the number of adatoms with R^4 for the cylindrical thermal spike. The linear dependence is plotted in the range of R where the viscous flow mechanism is dominant. A local linear dependence is revealed for short cylinders ($L < 4a_0$).

described by a linear dependence but the slope of the curve is half that for long cylinders. For these cylinders, the craters are always formed and defects of vacancy type are not observed.

IV. SIMULATION OF SURFACE INFLUENCE ON VACANCY LOOP YIELD

The influence of the surface on vacancy clustering in near-surface cascades has been simulated in the hybrid model for Cu and Cu_3Au . As discussed in Sec. III B, for cascade zones intersected by the surface, the additional number of vacancies can be calculated by Eq. (1), where parameters N_{sputt} , N_{add}^i , and N_{crat} are determined by MD modeling (see the data for $L = 8a_0$ in Fig. 9, for example). A table was constructed showing the results for N_{add}^V obtained for the combinations of T , L , and R used as the initial parameters in the MD simulations. At the moment in time when the melted cascade core intersected the surface, the average temperature and the number of melted cells at the surface were recorded. Using the tabulated data, the value of N_{add}^V was estimated by interpolation and added to the number of vacancies in the melt. After that the hybrid model¹ was used to simulate the cooling of the thermal spike and the density redistribution within it. Cascade collapse to form a vacancy loop was considered to occur in zones which achieved the critical values C_v^{cr} and N_v^{cr} discussed in Sec. II. Loops which had too few vacancies to achieve a size of at least 2 nm were not counted, in order to introduce a ‘‘resolution limit’’ to mimic experimental conditions.

Figures 14(a) and (b) show the calculated and experimentally measured vacancy loop yield as a function of depth of disordered zones in Cu and Cu_3Au , respectively, produced by irradiation with 50-keV Ni^+ ions at 373 K. The surface was inclined at 45° to the incident ion beam. For comparison the results of calculation of yield without including surface influence ($N_{\text{add}}^V = 0$) are also presented for Cu in Fig. 14(c). The calculated defect yield in Cu decreases from about 0.8 near the surface to 0.6 in the bulk. The calculated and experimental vacancy loop yield in Cu_3Au are very close to each other and decrease from about 0.7 just below the surface to 0.4 deeper in the foil. Figure 15 shows the loop size histogram for the Cu_3Au alloy.

V. DISCUSSION

In the modeling approach used here and in Ref. 1, local melting in the cascade core is required to form a vacancy loop by the process known as cascade collapse. If the melted core of a cascade intersects a surface, additional vacancies are generated in the core region as it recrystallizes, thereby increasing the probability of collapse and the size of the vacancy loop. The thermal spike model was used in the present paper to simulate the melting process beneath the surface. For an irradiated foil, the distribution with depth of cascades that intersect the surface gives a dependence of the yield on depth. The results of the simulations of surface influence on vacancy loop yield were obtained here for both Cu and Cu_3Au . The vacancy loop yield is predicted to be higher in the atomic layers close to the surface than in the interior volume because of the appearance of an additional popula-

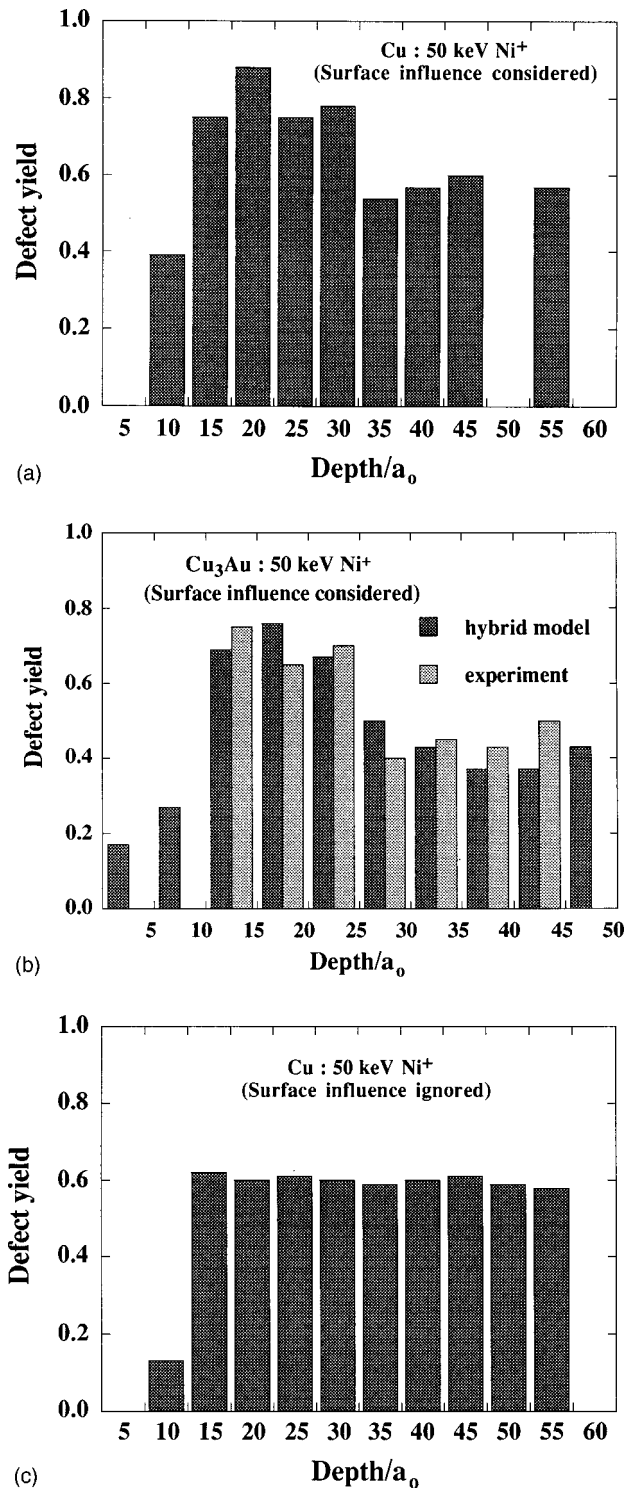


FIG. 14. The vacancy loop yield calculated by the hybrid model as a function of depth of zones in the foil for (a) Cu and (b) Cu₃Au irradiated with 50-keV Ni⁺ ions at an incident angle of 45°. For comparison, the results of the calculation of yield without including surface influence, i.e., $N_{\text{add}}^V = 0$, are also presented for Cu in (c).

tion of loops that should be visible in conventional transmission electron microscopy.

The mechanism of enhanced vacancy generation in the melted and recrystallized region of a cascade near a surface is based on combinations of two main processes. First, fast evaporation of atoms occurs at the end of the collisional

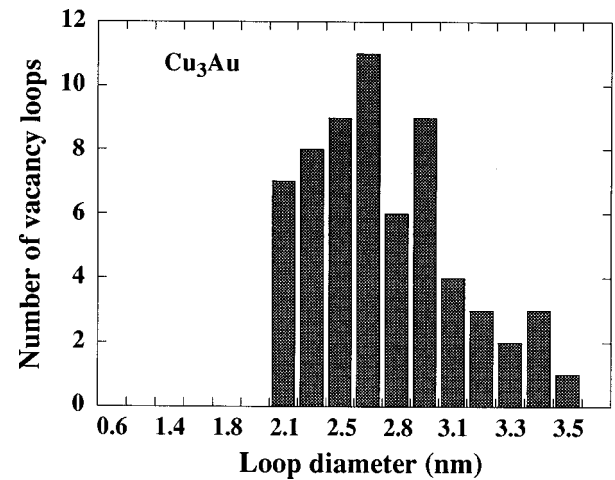


FIG. 15. Calculated size distribution of vacancy loops for Cu₃Au.

phase when the thermalization processes in the thermal spike are developed. At this stage, some atoms escape from the surface and a crater is formed. As time proceeds, liquid emerges from the deeper layers through the process of viscous flow of the melt towards the surface. Part of the liquid can flow onto the surface forming adatoms, thereby increasing the number of vacancies in the solid that can condense into a vacancy dislocation loop.

For typical temperatures in the thermal spike (5000–10 000 K) the number of additional vacancies N_{add}^V in the recrystallized region and the size of the crater at the surface are dependent mainly on the size of the melted spot at the surface and the shape and size of the liquid region under it. It was demonstrated by the hybrid model in Sec. III that although the melted zone of cascades in Cu or Cu₃Au produced by 50-keV Ni⁺ ions can have complicated shapes, generally the melted volume close to the surface can be approximated by a cylindrical or spherical geometry. This has allowed the quantitative relationships between the number of additional vacancies and the dimensions of the melted zone to be estimated using a simplified geometry (cylinder or sphere) of the thermal spike within the restrictions of MD simulation.

It was shown by MD of a cylindrical thermal spike that N_{add}^V depends on the ratio $2\bar{R}/\bar{L}$, where \bar{R} is the average radius of the melted spot at the surface and \bar{L} is the average length of the cylinder. If the ratio $2\bar{R}/\bar{L}$ is larger than one, N_{add}^V tends towards zero and only a crater is formed at the surface with no loop formation. The result is the outcrop of almost all the liquid at the surface. A collapsed, extended vacancy defect in the resolidified metal was registered only in cases when the ratio $2\bar{R}/\bar{L}$ was less than unity and the cylinder length was more than $4-5a_0$.

The melted zones of cascades that intersect the surface of Cu and Cu₃Au irradiated by 50-keV Ni⁺ ions have an average length of melted region of about $7-8a_0$, and MD calculations were used for these zones to obtain the relationships used in the hybrid model to investigate the nucleation of vacancy loops. By using this hybrid continuum/MARLOWE model, approximately 100 cascades were simulated for each metal and this has allowed us to derive the distribution of

melted zones and loops (and therefore the vacancy loop yield) as a function of depth. In spite of the simplification of the approach used, the comparison of calculation with experiment has demonstrated a very good agreement. The good fit of the calculated and experimental defect yields can be easily understood if we take into account the physics of surface influence which has been revealed by the MD simulations and incorporated into the hybrid model. The modified model simply increases the number of vacancies in the melted region crossed by the surface. Even if the additional number N_{add}^V is overestimated in the simplified geometry of the MD calculation, the model is insensitive to small changes in N_{add}^V and the final value of loop yield is little affected. An error in N_{add}^V would affect the size distribution of visible loops, but unfortunately the experimental distribution of loop size is not available for direct comparison with the calculated one. However, the data of Fig. 15 are in a reasonable agreement with the distribution for nickel obtained in Ref. 15

Gao and Bacon⁸ and de Diego and Bacon¹⁶ have shown by MD simulation of cascades in Ni₃Al and Zr that far fewer self-interstitials survive in cascades near a surface. This is due to a combination of collisional and diffusive effects. However, the model used in the present work does not include the mechanism of annihilation of interstitial atoms and small glissile interstitial clusters by diffusion to the surface. These are expected to reduce vacancy-interstitial recombination in cascades near a surface and so possibly enhance vacancy loop production. This mechanism was discussed by Muller *et al.*⁴ and invoked by them to explain their experimental finding of increasing vacancy loop yield for cascades lying at depths larger than 5–10 nm. They considered that the cascades at this depth have no obvious connection to the surface and cannot be influenced by it through the intersection with melted zones. We have demonstrated here by the hybrid model simulation that there are parts of cascades among the total population at this depth which should have direct connection to the surface.

Gao and Bacon⁸ concluded that the main mechanism for export of atoms to the surface is a collisional process, rather than viscous flow. That conclusion was based on the MD simulation of 10 keV cascades in Ni₃Al. For cascades with

energy 50 keV and higher the mechanism of additional vacancy generation is more complicated and includes both the fast evaporation of atoms and viscous flow. In the timespan of a cascade, the collisional process and fast evaporation occur almost simultaneously and it is difficult to separate them in direct MD cascade simulations. As emphasized earlier, the contribution of different mechanisms depends on the depth of the melted zone, the average temperature in it and the size of the melted spot at the surface.

VI. SUMMARY

A model of vacancy cluster nucleation in a displacement cascade near a surface has been proposed. The surface influence has been included in the model simply by the procedure of additional vacancy generation in a melted cascade core intersected by the surface. Information concerning the geometry of such melted regions for Cu and Cu₃Au irradiated by 50-keV Ni⁺ has been obtained by using a hybrid continuum/binary-collision model developed previously.¹ This was then used to formulate an MD study of the mechanisms of surface influence on vacancy generation. The MD simulations enabled us to obtain data for the number of atoms either sputtered from, or added to, the surface intersected by a melted zone. From these data, the relationship between the number of additional vacancies and the size and shape of a zone was determined. This number was then used in the hybrid model to calculate the vacancy dislocation loop yield as a function of depth for Cu and Cu₃Au. The loop yield increases just below the surface, an effect due to the appearance of extra vacancies in the melted and recrystallized volume of a cascade through the mechanisms of thermal sputtering and viscous flow of atoms from the melt. The results of the calculations are in good agreement with experiment.

ACKNOWLEDGMENTS

This research was supported by an INTAS Grant (INTAS-93-3454-ext). Valuable discussions with Dr. A. F. Calder, Dr. F. Gao, and Dr. M. L. Jenkins are gratefully acknowledged.

¹V. G. Kapinos and D. J. Bacon, Phys. Rev. B **52**, 4029 (1995).

²M. L. Jenkins, K. H. Katerbau, and M. Wilkens, Philos. Mag. A **34**, 1141 (1976).

³M. L. Jenkins and M. Wilkens, Philos. Mag. A **34**, 1155 (1976).

⁴S. Muller, M. L. Jenkins, C. Abromeit, and H. Wollenberger, Philos. Mag. A **75**, 1625 (1997).

⁵M. Ghaly and R. S. Averback, Phys. Rev. Lett. **72**, 364 (1994).

⁶R. S. Averback and M. Ghaly, Nucl. Instrum. Methods Phys. Res. B **90**, 191 (1994).

⁷M. Ghaly, R. S. Averback, and T. Diaz de la Rubia, Nucl. Instrum. Methods Phys. Res. B **102**, 51 (1995).

⁸F. Gao and D. J. Bacon, Philos. Mag. A **75**, 1603 (1997).

⁹M. T. Robinson, computer code MARLOWE, Oak Ridge National Laboratory, 1992.

¹⁰M. W. Finnis, P. Agnew, and A. J. E. Foreman, Phys. Rev. B **44**, 567 (1991).

¹¹V. G. Kapinos and D. J. Bacon, Phys. Rev. B **53**, 8287 (1996).

¹²V. G. Kapinos and D. J. Bacon, Philos. Mag. A **72**, 1413 (1995).

¹³G. J. Ackland and V. Vitek, Phys. Rev. B **41**, 10 324 (1990).

¹⁴H. F. Deng and D. J. Bacon, Phys. Rev. B **48**, 10 022 (1993).

¹⁵I. M. Robertson, J. S. Vetrano, M. A. Kirk, and M. L. Jenkins, Philos. Mag. A **63**, 29 (1991).

¹⁶N. De Diego and D. J. Bacon, Radiat. Eff. Defects Solids **141**, 337 (1997).

¹⁷V. G. Kapinos and D. J. Bacon, Philos. Mag. A **68**, 1165 (1993).